ELSEVIER

Biophysical Chemistry 126 (2007) 25–35

Biophysical Chemistry

http://www.elsevier.com/locate/biophyschem

Elimination of the C-cap in ubiquitin—structure, dynamics and thermodynamic consequences☆

Dmitri N. Ermolenko [a,c,1], Bindi Dangi [b,d,1], Anzor Gvritishvili [a], Angela M. Gronenborn [b,*], George I. Makhatadze [a,*]

[a] *Department of Biochemistry and Molecular Biology, Penn State University College of Medicine, Hershey, PA, United States*
[b] *Laboratory of Chemical Physics, NIDDK, NIH, Bethesda, MD, United States*
[c] *Bach Institute of Biochemistry, Russian Academy of Sciences, Moscow 119071, Russia*
[d] *Martek Biosciences, 6480 Dobbin Road, Columbia, MD 21045, United States*

Received 14 February 2006; received in revised form 22 March 2006; accepted 22 March 2006
Available online 5 April 2006

Abstract

Single amino acid substitutions rarely produce substantial changes in protein structure. Here we show that substitution of the C-cap residue in the α-helix of ubiquitin with proline (34P variant) leads to dramatic structural changes. The resulting conformational perturbation extends over the last two turns of the α-helix and leads to enhanced flexibility for residues 27–37. Thermodynamic analysis of this ubiquitin variant using differential scanning calorimetry reveals that the thermal unfolding transition remains highly cooperative, exhibiting two-state behavior. Similarities with the wild type in the thermodynamic parameters (heat capacity change upon unfolding and *m*-value) of unfolding monitored by DSC and chemical denaturation suggests that the 34P variant has comparable buried surface area. The hydrophobic core of 34P variant is not packed as well as that of the wild type protein as manifested by a lower enthalpy of unfolding. The increased mobility of the polypeptide chain of this ubiquitin variant allows the transient opening of the hydrophobic core as evidenced by ANS binding. Taken together, these results suggest exceptional robustness of cooperativity in protein structures.

Keywords: Protein structure; Protein stability; Cooperativity of unfolding; Differential scanning calorimetry; Heteronuclear NMR; Circular dichroism spectroscopy

1. Introduction

Understanding the relationship between the linear amino acid sequence, the 3D structure and the thermodynamic stability of a protein still remains elusive. In an effort to elucidate the underlying principles it is particularly interesting to analyze cases in which a single amino acid substitution results in significant changes in the 3D-structure and/or stability.

Recently, the role of helix-capping interactions for protein structure and stability was explored by investigating the effects of amino acid substitutions at the C-cap position of the α-helix of ubiquitin. The single α-helix in ubiquitin comprises residues 24–33 and consists of three helical turns. The first residue proceeding the helix (C-cap residue) in the wild type ubiquitin is E34. Effects of amino acid substitution with all 20 naturally occurring amino acid at the C-cap on the stability of the ubiquitin variants revealed a number of interesting properties [1]. First, it was observed that stability changes correlate with the hydrophobic nature of residue 34. Second, far-UV CD and HSQC NMR experiments revealed no dramatic structural changes for all but one (Pro) amino acid substitution. Third, the Pro substitution in position 34 resulted in significant perturbations in the far-UV CD and HSQC NMR spectra, suggesting structural rearrangements in this ubiquitin variant. Here we report the results of the 3D structure determination of the 34P variant of ubiquitin using multidimensional

☆ Structure submission information: The structure has been deposited and assigned the RCSB ID code rcsb033194 and PDB ID code 1ZW7.

* Corresponding authors. A.M. Gronenborn is to be contacted at Laboratory of Chemical Physics, NIDDK, NIH, Bethesda, MD, United States. G.I. Makhatadze, Department of Biochemistry and Molecular Biology, Penn State University College of Medicine, Hershey, PA 17033, United States. Tel.: +1 717 531 0712; fax: +1 717 531 7072.
E-mail address: makhatadze@psu.edu (G.I. Makhatadze).

[1] These authors contributed equally to this work.

0301-4622/$ - see front matter © 2006 Elsevier B.V. All rights reserved.
doi:10.1016/j.bpc.2006.03.017

heteronuclear NMR spectroscopy. In addition, the thermodynamic properties of the 34P variant were characterized by differential scanning calorimetry (DSC), chemical denaturation and fluorescence spectroscopy. A significant change in the protein structure is observed that involves conformational changes at the C-terminus of the α-helix of ubiquitin. The structural changes of this ubiquitin variant are accompanied by peculiar changes in the thermodynamic properties of the protein, possible sources of which are discussed.

2. Materials and methods

2.1. Protein mutagenesis, expression and purification

Mutations in the ubiquitin gene were introduced using QuickChange site directed mutagenesis kit. The presence of the desired mutations was confirmed by sequencing the entire gene. Proteins were expressed from plasmid carrying the ubiquitin gene under control of the T7 promoter in BL21(DE3) or JM109 (DE3) and purified as described previously [1]. Protein concentration was measured spectrophotometrically using a molar extinction coefficient of 1480 at 276 nm [1]. Correction for the light scattering was done as described [2].

2.2. Circular dichroism

CD spectra were measured at 25 °C on a Jasco J-715 spectrophotometer as described elsewhere [1]. Each spectrum was the result of averaging five individual spectra using 0.1 cm cylindrical quartz cell. The protein concentration in all cases was 0.4 mg/ml in 30 mM glycine pH 3.5. Measured values of the ellipticity, Θ, were converted into the ellipticity per amino acid residue base, [3] as:

$$[\Theta] = \frac{\Theta \cdot \mathrm{MW_R}}{l \cdot c} \quad (1)$$

where l is the optical length of the cell, c is the concentration of the protein, and $\mathrm{MW_R}$ is the average mass of the amino acid residues taken to be 114 Da.

Urea-induced unfolding experiments were performed in 5 mM glycine/HCl, pH 3.5 by monitoring the changes in ellipticity at 222 nm. Changes in urea concentration in solution were achieved using an automated titration system based on a Microlab 500 dispenser (Hamilton, Reno, NV) as described [4]. Analysis of the data was done according to the linear extrapolation model using nonlinear regression routines as described elsewhere [5].

2.3. Differential scanning calorimetry

DSC experiments were preformed on a VP-DSC (MicroCal, Northampton, MA) instrument at a scan rate of 90°/h. All experiments were carried out in 30 mM glycine or sodium acetate buffers. The protein concentration in the DSC experiments varied between 1.5 and 3.5 mg/ml. All temperature-induced unfolding transitions were reversible as judged by the area under the excess heat capacity function of first and second scans. Calorimetric profiles were analyzed according to a two-state transition model using the nonlinear regression routine NLREG and in-house written scripts [6].

2.4. Fluorescence spectroscopy

Steady-state fluorescence experiments were performed on a FluoroMax Spectrofluorimeter with DM3000F software (SPEX Industries, Inc.) as described [7,8]. A constant temperature in the thermostated cell holder (25 °C) was maintained using a circulating water bath. A quartz cell with a 1 cm path length was used. The buffer used in all titration experiments and in measurements of fluorescence emission spectra was 25 mM sodium acetate, pH 5.5. Concentration of the stock solution of ANS (8-anilino-1-naphtalene sulfonic acid) in buffer was determined spectrophotometrically using an extinction coefficient of 5000 M^{-1} cm^{-1} at 355 nm [9]. Stock solutions of protein and ANS were mixed to the final concentrations 10 μM and 25 μM, respectively. All experiments were run in triplicate, intensity was corrected for dilution, and average values are reported. The excitation wavelength used was 350 nm.

2.5. NMR data acquisition

Isotopically labeled proteins (^{15}N and $^{15}N/^{13}C$) were prepared using MOPS based minimal media with ^{15}N-ammonium chloride and ^{13}C-glucose as the only source of nitrogen and carbon, respectively [1,2,10]. Ubiquitin samples for NMR experiments were prepared by dissolving the lyophilized protein samples in 5% acetic acid with subsequent dialysis against 30 mM acetate buffer, pH 5.0. NMR experiments were carried out on samples containing 1–2 mM of suitably labeled protein. All spectra were recorded at 25 °C on Bruker DMX600 or DMX500 instruments equipped with a triple-resonance, triple-axes gradient probe. Backbone assignments of the protein were based on ^{1}H-^{15}N-HSQC, 3D-HNCACB, CBCA(CO)NH, HNCA, HNCO, and HBHA(CO)NH spectra [11] and H(CCO)NH-TOCSY and C(CO)NH-TOCSY experiments [11–15] were used for side-chain assignments NOE assignments were made using a 3D-^{15}N NOESY-HSQC [16] and a 3D NN-NOESY-TROSY-HMQC experiments. Residual dipolar coupling data were obtained for ^{15}N and ^{15}N,^{13}C labeled protein samples using two alignment media. The first medium contained 5% of dodeca-alkyl-penta(ethylene glycol) and hexanol, with a molar ratio of the glycol derivative to hexanol of 0.96 [17]. The second alignment medium was a 6% polyacrylamide gel (5.4 mm stretched in a 4.1-mm internal diameter NMR tube) containing 36% w/v acrylamide, 0.92% w/v *N*,*N*′-methylene bisacrylamide (ratio 39:1) [18]. One-bond ^{15}N–$^{1}H(N)$ and ^{15}N–$^{13}C'$ and two-bond $^{13}C'$–$^{1}H(N)$ dipolar couplings were measured using sensitivity-enhanced E-COSY-type HSQC experiments [19]. One-bond $^{13}C_\alpha$–$^{13}C'$ and $^{1}H_\alpha$–$^{13}C_\alpha$ dipolar couplings were measured using 3D-$^{13}C'$-coupled/^{1}H-decoupled HNCO and 3D ^{1}H-coupled HCA(CO)N experiments, respectively. Identical samples without the alignment media were used to collect reference

spectra and the residual dipolar couplings were calculated as a difference in the values measures with and without the alignment media. Da and R were estimated by analysis of the histograms using the method described by Brunger et al. [20]. The program PALES [21] was used to assess the differences in the observed dipolar couplings and those calculated, using the NMR structure of wild-type human ubiquitin. Relaxation data were collected on a ^{15}N-labeled sample at a single field strength (500.13 MHz) at 25 °C. Spin-lattice relaxation time constants (T_1), spin–spin relaxation time constants (T_2) and ^{15}N{^{1}H}NOE values for backbone ^{15}N nuclei were measured by 2D inverse-detected methods using pulse sequences described by Kay et al [22]. Water flip back methods were used for solvent suppression [23]. All spectra were acquired with $1024\cdot(\mathrm{HN})\times 256\cdot(^{15}\mathrm{N})$ complex points and spectral widths of 7002.801 Hz and 1317.783 Hz in the HN and ^{15}N dimensions, respectively. Points were obtained in random order for both the T_1 and the T_2 relaxation experiments using 16 transients per point and a recycle delay of 2 s. The optimum recycle delay was set to ~3 times the T_1 value of the amide protons. The relaxation delays employed for the T_1 experiments were 16, 160, 320 640, 960, 1200 ms and those used for the T_2 experiments were 8, 16, 32, 64, 128, 160, 240 ms. The ^{15}N{^{1}H}NOE experiments consisted of two interleaved experiments. A pre-saturation period of 3 s was employed in the NOE experiment consisting of 135° pulses applied every 30 ms. Deuterium exchange experiments were carried out on a lyophilized sample dissolved in 30 mM sodium acetate buffer, pH 5.0, 100% D_2O and ^{1}H–^{15}N-HSQC spectra were recorded at suitable intervals over a period of 24 h at 25 °C.

2.6. NMR data processing and analysis

All NMR data were processed using the nmrPipe suite of programs and analyzed using the Pipp package [24]. Heteronuclear dimensions were extended by linear prediction and zero filled prior to Fourier transformation. Square cosine window functions were applied with optimized shifts to all the data sets. T_1 and T_2 relaxation time constants were estimated by fitting intensities of the cross-peaks to a single exponential decay curve and uncertainties in relaxation parameters were ascertained from Monte Carlo simulations. Values for steady state NOEs were calculated based on ratio of intensities of peaks in the spectra recorded with and without proton saturation. Errors in these ratios were estimated from baseline noise in the two spectra. Residues involved in conformational exchange were identified based on criteria described by Tjandra et al. [25]. Secondary structure analysis was carried out using the CSI program [26] and ϕ/ψ angles were predicted using C_α, C_β, C′, H_α and ^{15}N chemical shifts in TALOS [27].

2.7. Structure calculations

NOE cross-peaks were classified as strong, medium, weak or very weak by qualitative inspection. Upper limits for inter-proton distance-constraints of 3.0, 4.0, 5.0 and 5.5 Å were used for these categories, respectively. Only HN–HN, HN–H_α, and few HN–methyl–proton restraints were used. For methyl protons, corrections of 1 Å were applied. Backbone ϕ and ψ angle constraints were calculated using TALOS as described above and only predictions classified as "good" were used in the calculations. Ranges for dihedral angle constraints were based on errors predicted for the ϕ and ψ values by TALOS. Although several residual dipolar couplings were determined, the final protocol used only ^{1}H–^{15}N, and ^{13}C–^{13}C′ residual dipolar couplings, since addition of the other residual dipolar couplings did not improve the quality of the structure significantly. This is most likely due to the redundancy in information associated with some of these couplings. The final input data therefore consisted of backbone NOEs, ϕ and ψ angles, C_α, C_β and H_α chemical shifts and dipolar coupling values. Table 1 lists all restraints used in the structure calculation. The average energy-minimized structure from the ensemble of 1D3Z (after introduction of the appropriate mutations) was used as the starting structure. In addition, a helix was introduced at the C-terminus of the starting structure (residues 76–82) using the swisspdb viewer [28]. This was implemented to test for any bias in the protocol towards the starting structure. Structure calculations were performed using CNS version 1.0 [20] on an SGI platform. The refinement protocol for annealing involved torsion angle heating (100 K, 1000 steps) followed by cooling in torsion (100 K, 5000 steps) and Cartesian space (1000 K, 10,000 steps). The dipolar coupling force constant was ramped from 0.01 to 1.0. The quality of the structures was analyzed using PROCHECK-NMR [29]. Figures were generated using MOLMOL [30].

2.8. Light scattering

Light scattering data were obtained using an analytical superdex-75 column (1.0 × 30 cm; Amersham Biosciences, Piscataway, NJ) with in-line multi-angle light scattering (DAWN EOS, Wyatt Technology, Inc.) and refractive index

Table 1
Experimental restraints used for structure calculations

(1) NOE	137
HN–HN	
Sequential	27
Medium-range	3
Long-range	3
HN–H_α	
Intra-residue	45
Sequential	20
Medium-range	14
Long-range	23
HN–Methyl	
Intra-residue	1
Sequential	1
Long-range	0
(2) Dihedral angles	90
ϕ	43
ψ	47
(3) Dipolar couplings	276
HN (gel)	61
HN (PEG)	67
C_αCO (gel)	74
C_αCO (PEG)	75

detectors (OPTILAB DSP, Wyatt Technology, Inc., Santa Barbara, CA). 60 μg of protein in 75 μL of 30 mM acetate buffer, pH 5.0, containing 0.02% sodium azide was applied to the pre-equilibrated S75 column at a flow rate of 0.5 ml/min at room temperature and eluted with the same buffer. The $34P^{\#AAA}$ variant of ubiquitin eluted as a single peak corresponding to a monomer molecular mass species (9.8 kDa).

2.9. Surface area calculations

Water accessible surface area ASA was calculated using NACCESS software package [31]. Calculations were carried out using van der Waals radii of Chothia [32], and a probe size of 1.4 Å. For the NMR structures, calculations were performed for the individual models and the average values are reported. The unfolded state structure was modeled as an extended chain comprising the appropriate amino acid sequence.

3. Results and discussions

3.1. Circular dichroism analysis of the position 34 ubiquitin variants

The α-helical C-cap position is defined as the first residue following a helix, exemplified by non-helical torsional angles [3]. Statistical analysis of the frequencies of occurrence of different residues at this position based on experimentally determined structures in the Protein Data Bank reveals that the amino acid with the lowest propensity is Pro [3,33,34]. This is easily understood since a Pro residue imposes significant constraints on the conformation of its preceding residue. In particular, any residue before a Pro cannot adopt a helical backbone conformation without significant strain [35]. Therefore, the 34P substitution in the C-cap position of the α-helix in ubiquitin is expected to force residue 33 out of the helical ϕ/ψ conformation. Such disruption of the helical structure is consistent with the observed changes in the CD spectrum for the E34P variant (Fig. 1), including the possibility that these structural changes propagate with pronounced effects on the remaining residues in the helix. In order to evaluate the effect of the local environment on the proline substitutions, this substitution was also introduced into a different background, namely WT^{AAA} (see Fig. 2). In the WT^{AAA} variant, residues in positions 11, 32, and 33 that are located in the immediate vicinity of residue 34 were substituted by Ala [1]. Position 11 in the WT sequence is a lysine, forming a salt bridge with Glu34 [4] and positions 32 and 33 are Asp and Lys residues, respectively. The stability of this alanine substituted variant, WT^{AAA}, is several kJ/mol higher than that of WT [1]. Despite these sequence changes, the $34P^{AAA}$ variant of ubiquitin exhibits similar CD spectrum to that of 34P, albeit a very different one compared to the CD spectra of all other non-proline position 34 variants (Fig. 1).

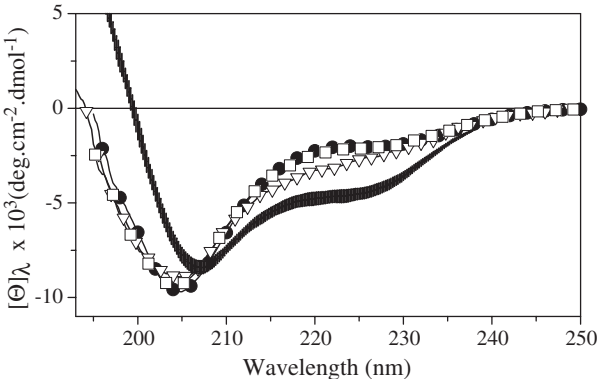

Fig. 1. Far UV-CD spectra of the ubiquitin variants: $34P^{\#AAA}$ (●), $34P^{AAA}$ (□), 34P (▽). The solid line is a representative reference spectrum for all non-Pro substitutions at position 34, with the thickness defined by the standard deviation in the ellipticity at a given wavelength obtained for the different non-Pro variants.

One possible explanation for the observed significant changes in the CD spectrum of the 34P variant is the fact that this variant is the least stable protein of all position 34 variants [1]. This could result in protein sample which contains a mixture of folded and unfolded species and thus yielding a reduced CD signal. However, we believe this is an unlikely scenario, since other substitutions at position 34 (e.g. 34K [1]) that are almost equally destabilizing do not show such loss of ellipticity in the CD spectra. Nevertheless, in order to completely eliminate the reduced stability as a major factor responsible for the changes in the CD spectra of the 34P variants, we created the $WT^{\#AAA}$ background (see Fig. 2) with an additional stabilizing substitution, R42E, that increases the melting temperature by ~13 °C [36]. A comparison of the thermal unfolding profiles for the 34P variants in the different backgrounds as monitored by DSC is shown in Fig. 3. As it can be appreciated, the $34P^{\#AAA}$ variant is fully folded at pH 3 and room temperature. However, the CD spectrum of this stabilized variant is very similar to the other less stable 34P variants (Fig. 1). It therefore seemed clear that the changes in the CD spectra were not directly related to protein stability but reflected conformational changes in the folded structure. In order to characterize these global conformational changes we determined the 3D-structure of the $34P^{\#AAA}$ ubiquitin variant by NMR spectroscopy.

3.2. NMR investigations—chemical shift assignment and comparison with the wild-type protein

Since chemical shifts are extremely sensitive parameters reporting on the particular structural and electronic environment around the respective atoms, assessment of structural identity and similarity can be easily conducted by NMR, even prior to a complete structure determination. Closely similar resonance frequencies of amide groups provide a reliable measure for similarities in overall structure for related proteins or variants and this property can be exploited for fast and efficient screening of mutant libraries by NMR [37]. A comparison between the chemical shifts (^{15}N and HN) for the variant and wild-type yeast ubiquitins shows several important differences (see Fig. S1 in electronic supplement). Amino acid changes in the $34P^{\#AAA}$ variant with respect to the wild-type protein are K11A, D32A, K33A, E34P, R42E and R63K and visual

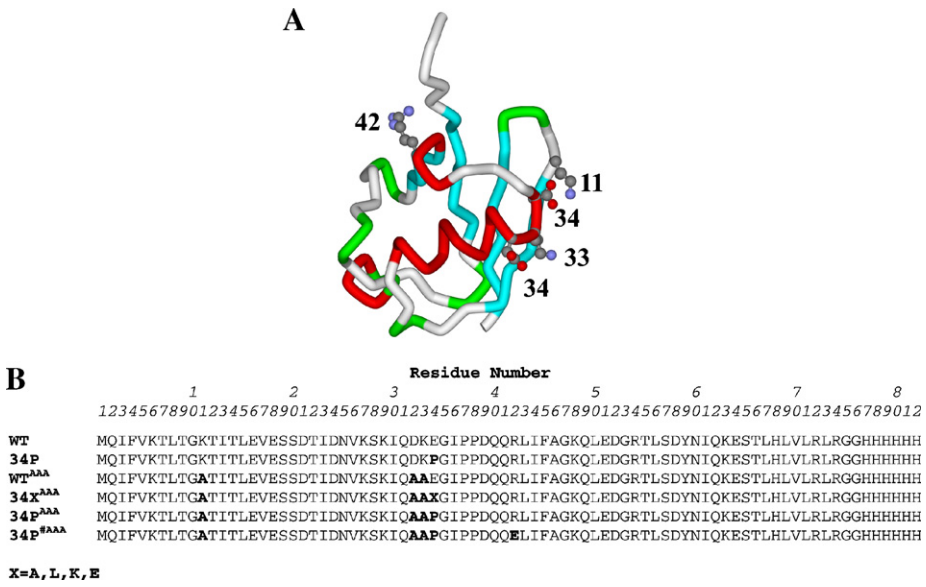

Fig. 2. Ubiquitin variants. (A) Backbone representation of the ubiquitin molecule depicting those residues that were substituted in the different variants. (B) Amino acid sequences of the ubiquitin variants used in this study. Changes are indicated in bold.

inspection (see Figs. S1A and S1B in electronic supplement) reveals that the majority of chemical shift changes reside in and around the location of the amino acid substitution, primarily in the center of the helix. The largest differences are observed for residues 28, 30, 32, 33 and 36 (up to ~1.5 ppm for ^{1}H and ~10 ppm for ^{15}N. As reference, ^{15}N chemical shift differences between the WT and the 34A^{AAA} variant were compared (see Fig. S1C in electronic supplement). This variant contains all the amino acid substitutions present in 34P$^{\#AAA}$, except for E34P, which is an Ala and R42E, which remains the wild type Arg. Chemical shift differences for this variant are minimal, compared to wild-type protein, particularly in the helix (residues 23–34), despite the substitutions at positions 32 and 33. This clearly identifies the E34P substitution as the primary cause for the observed changes in the helical residues. In addition, the 34P$^{\#AAA}$ variant also displays small, but noticeable chemical shift differences for the backbone amides at positions 11 and 12, most likely caused by the K11A substitution. In the wild-type protein structure, the side chains of E34 and K11 are involved in a salt bridge. Naturally this interaction will be absent in the variant. Indeed, the structure of the variant (see below) reveals that the conformation of residues around position 11, specifically the loop containing residues 8, 9 and 10 is slightly altered, a structural change that is transmitted to residues in the environment of amino acid 70 and other residues in that region (residues 69–71). Similar chemical shift changes are also observed in the 34A^{AAA} variant, supporting the notion that these differences (at 11, 12, 69–71) are not the result of the E34P substitution. Other areas that display chemical shift differences comprise residue 53 and the C-terminus. The chemical shift of G53 could be affected by the orientation of the helix and this is discussed in more detail below. Differences observed for the C-terminal residues are most likely caused by the presence of the six-histidine tag.

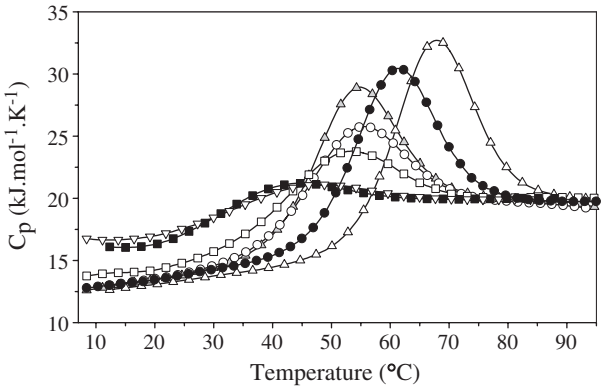

Fig. 3. DSC profiles of the ubiquitin variants: 34P$^{\#AAA}$ (○, pH 3.0), 34P (□—pH 3.5, ■—pH 3.0), 34P^{AAA} (▽—pH 3.0), 34A^{AAA} (△—pH 3.0; ▲—pH 2.25), and WT (●). Solid lines represent the fit of the experimental data to a two-state model.

3.3. Secondary structure of the 34P variant

The analysis of secondary chemical shifts was performed using the programs CSI and TALOS (see Fig. S2 in electronic supplement). The most notable difference between the secondary structure elements observed in WT ubiquitin and the 34P$^{\#AAA}$ variant is the loss of helical structure for residues from 29 through 34. For the present data set, TALOS resulted in good predictions for 60% of the residues, consistent with the normal performance of this program. However, given the fact that even for "good" predictions the possibility of errors exists (average error of ~3%), we corroborated the TALOS results for all residues using additional information, namely deuterium exchange rates and NOEs. A comparison between the ϕ/ψ angles in the wild-type protein (1D3Z structure) and the ϕ/ψ

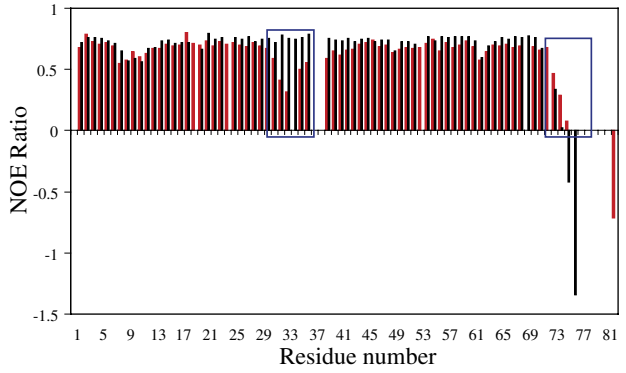

Fig. 4. Comparison of heteronuclear $^{1}H–^{15}N$ NOE ratios. The red bars represent values calculated for the $34P^{\#AAA}$ variant and the black bars are those reported for wild-type human ubiquitin. Residues exhibiting major differences are boxed in blue.

angles predicted by TALOS for the $34P^{\#AAA}$ variant reveals that the only residue that exhibits a significant difference is residue 33, with ϕ/ψ −96/116 for the variant (A33) and −94/−24 for the wild-type (K33). The differences between the backbone angles of all other residues in the $34P^{\#AAA}$ variant, compared to the wild-type, are within 2 standard-deviations of the predictions made by TALOS, clearly indicating similar conformations.

3.4. Dynamic behavior of the 34P variant

Relaxation measurements, T_1, T_2 and ^{15}N heteronuclear NOEs, were carried out for the $34P^{\#AAA}$ variant and compared to WT ubiquitin. Analysis of the T_1 and T_2 data yielded a correlation time consistent with a monomeric species. For residues 18, 19, 24 and 48, additional conformational exchange contributions were noted. ^{15}N heteronuclear NOE values for the wild-type human protein at 27 °C and for the $34P^{AAA}$ variant at 25 °C are presented in Fig. 4. Residues for which a drastic reduction in the heteronuclear NOE values was observed, are located in the middle of the helix and at the C-terminus. Such low values indicate that the backbone amides of these residues have to exhibit significant motions on a fast timescale. This also suggests that these residues are not involved in forming rigid, well-defined secondary structure elements (α/β). Hydrogen–deuterium exchange experiments confirmed these observations. In particular, most of the amide resonances corresponding to regular secondary structure elements as predicted by TALOS remained as strong peaks in the ^{15}N-HSQC spectrum following exchange for 2 h in 100% D_2O buffer. On the other hand, resonances located in loops and corresponding to the last two turns of the helix in the WT structure, except residue 30, were either very weak or absent.

3.5. Structure of the 34P variant

Structure calculations were carried out as described under Materials and methods. A preliminary analysis of the residual dipolar couplings was carried out for the $^{1}H–^{15}N$ values obtained on the ^{15}N labeled 34P variant sample in the polyethylene glycol media, using the program PALES. The average minimized structure from the 1D3Z ensemble was used as the reference structure. It should be pointed out that the backbone RMSD for the ensemble of structures for residues 2–71 is 0.09 Å, making the average minimized structure very similar to any of the structures within the ensemble. Fig. 5 displays the correlation between the predicted and the observed dipolar couplings for the current data set, exhibiting a R^2 value of 0.76 and the Q factor of 0.5. Outliers in the correlation are easily identified and arise from residues 9, 11, 30–33, 35, 36, 39, 40, 75 and 76. Note that residues 34, 37, 38 are prolines and therefore no $^{1}H–^{15}N$ dipolar coupling data can be obtained. The data for residues 77–82 cannot be included since this part of the polypeptide chain is absent in the reference structure. Disregarding the outliers form the correlation results in a R^2 value of 0.96 and a Q factor of 0.2. Therefore, the primary difference in the structure of the variant compared to the wild-type protein is confined to the region comprising residues 30–40, with the remainder of the backbone structure being very similar. This conclusion is corroborated and substantiated by the structure calculations for the $34P^{\#AAA}$ variant. The family of the top 20 structures is displayed in Fig. 6. For well-defined secondary structure regions (residues 2–7, 13–30, 40–72) this ensemble exhibits a backbone rmsd value of 0.61 Å. At this point we would like to emphasize that the final structural ensemble presented here is not biased towards the secondary-structure elements in the starting structure. As detailed in Materials and methods, we introduced a helix at the C-terminus (residues 77–82) in the starting structure, to serve as an internal control. The corresponding C-terminal residues in the final structure assume random coil conformations, clearly different from the starting conformation, demonstrating that the starting conformation does not influence the final structure. Analysis of the final structure using Procheck shows that 80% of the residues are within the most favorable region of the Ramachandran plot and that no residue lies in disallowed regions. Structural comparison between the wild-type and the

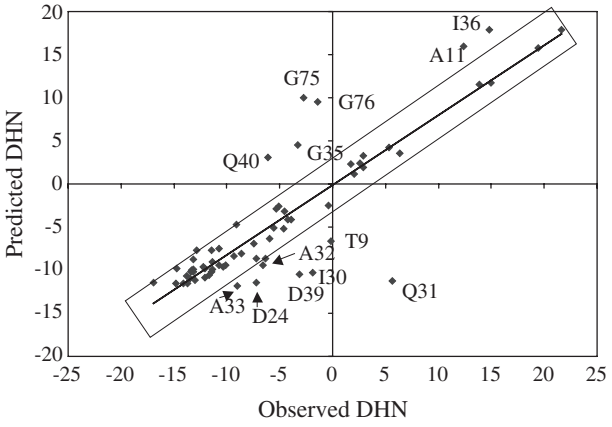

Fig. 5. Correlation between predicted and observed one-bond residual dipolar $^{1}H–^{15}N$ couplings. The experimental couplings were determined for the ^{15}N labeled $34P^{\#AAA}$ variant at 25 °C and predicted DHN values were calculated for the 1D3Z structure using the program PALES. Values for selected amino acids are labeled by residue name and number.

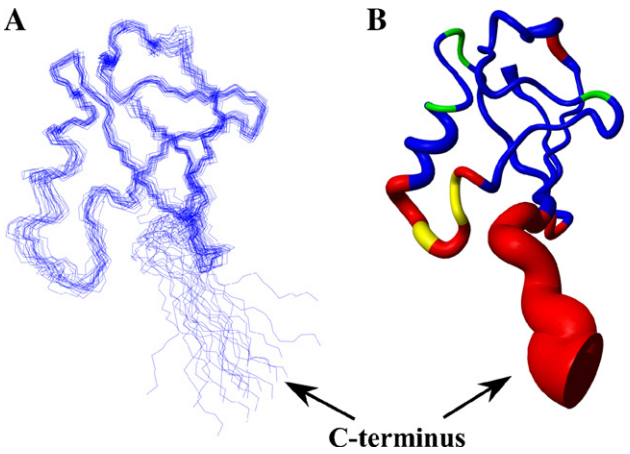

Fig. 6. Structure of the 34P$^{\#AAA}$ variant. (A) Ensemble of the top 20 structures showing the backbone atoms only. (B) Schematic representation of the structure depicting motional properties: residues exhibiting high mobility and conformational exchange are marked in red and green, respectively. The diameter of the tube is proportional to the RMSD of the ensemble. Proline residues are marked in yellow and no relaxation data is available for these.

34P$^{\#AAA}$ variant structure reveals an essentially identical overall fold, with the notable difference of a shortened helix in the variant structure and a somewhat more open or loose packing around this area. In the wild-type protein, the helix extends throughout residues 24–34 and side chain interactions are observed between helical amino acids and those in β-strand 2 (residues 12–16). If the same or very similar close packing were present in the variant structure, NOEs would be expected between the amide proton of residue 16 and the side chain protons of residue 29. These are clearly not seen in the 3D ^{15}N-NOESY-HSQC spectrum of the variant and despite extended efforts to observe such interactions. In fact, no NOEs were observed between any amide proton of residues 12–16 (β-strand 2) and any side chains proton of helical amino acids, suggesting that the local structure is less well packed and clearly more dynamic than the wild type structure Overall, the major difference in the variant structure appears to be a melting of the helix, caused by the loss of the capping interaction and an associated loss in H-bonding interactions. In particular, the wild type structure (1D3Z) contains characteristic α-helical hydrogen bonds between, 34HN–30CO, 33HN and 29CO, 32HN and 28CO, 31HN and 27CO for the last two turns of the helix which are clearly disrupted in the variant caused by the glutamate to a proline substitution. Local melting of regions within well-folded protein structures has been observed for other small proteins and RDC measurements are ideally suited to detect such 'melting hot-spots' [38].

The final structure ensemble as well as the dynamic properties of the 34P$^{\#AAA}$ variant structure are displayed in Fig. 6. The present structure is not as tightly packed as the WT protein and contains a noticeable hydrophobic crevice. Using the individual structural models we calculated the exposed surface area (ASA) upon unfolding to be 4210±390 Å^2 for the variant, while unfolding exposes 5780±280 Å^2 of surface area in the WT structure (Table 2). Thus, ca. 30% less surface area will become exposed upon unfolding of the 34P$^{\#AAA}$ variant protein. It is also notable that the standard deviation of the mean ASA is larger for the 34P$^{\#AAA}$ variant than for the wild type again suggesting an increased dynamic behavior. In this respect it is of interest to examine our variant structure in the light of a recent report on "NMR snapshots" of a fluctuating ensemble of ubiquitin [39]. These authors showed that under destabilizing conditions the helix can swing in and out of the compact structure by >3 Å with a simultaneous reorientation of the C-terminal segment, resulting in an "open" conformer. This conformer has strong similarities with our current variant structure, demonstrating the intrinsic ability of the ubiquitin fold to open up in a dynamical fashion.

3.6. Thermodynamics of the 34P variant

Despite these noteworthy changes in the three-dimensional structure, the thermal unfolding of the 34P variants remains highly cooperative and appears to follow a two-state model (Fig. 3). However, significant changes in the thermodynamic parameters of unfolding are observed. The 34P ubiquitin variants are very unstable. For example, 34P substitution in the WT background leads to a 9 kJ/mol decrease in stability relative to the 34A variant, while the 34P substitution in the WT^{AAA} background results in a 14 kJ/mol lower stability compared to the 34A^{AAA} variant [1]. Importantly, this decrease in stability is largely enthalpic (Fig. 7). This fact is easily appreciated by comparing the DSC profiles of the 34P ubiquitin variants (34P, 34P^{AAA} or 34P$^{\#AAA}$) and of the 34A^{AAA} protein (Fig. 3). When compared at the same temperature, the heat absorption peak for the 34A^{AAA} protein is larger than for 34P or 34P$^{\#AAA}$ variants, resulting in a lower enthalpy of unfolding (Fig. 3). The decrease in enthalpy of unfolding observed for the 34P variant is probably caused by decrease in the packing of 34P variant due to the decrease of interactions within the protein core. Conformational changes in 34P variant structure include residues I30, I36, that are involved in the formation of the hydrophobic core of ubiquitin, as previously identified by the Handel group [40,41].

Table 2
Solvent accessible surface areas for ubiquitin variants

	Structure				
	1UBQ	1UBI	1D3Z	34P	Unfolded
ASA_{npol}	2360	2340	2460±30	3630±120	6060
ASA_{pol}	2430	2450	2460±230	2860±270	4640
ΔASA_{npol}	3700	3720	3600±30	2430±120	
ΔASA_{pol}	2210	2190	2180±230	1780±270	
$\Delta C_{p,pred}$(MF)	4.5	4.6	4.4±0.3	2.6±0.5	
$\Delta C_{p,pred}$(SLR)	3.7	3.7	3.5±0.2	2.2±0.3	
$\Delta C_{p,pred}$(MSP)	3.5	3.5	3.4±0.1	2.2±0.2	
$\Delta C_{p,pred}$(MP)	4.1	4.2	3.9±0.3	2.2±0.4	
$\Delta C_{p,exp}$			3.3±0.3	3.2±0.4	

All ASA values are in Å^2 and all ΔC_p values are in kJ/(mol K). $\Delta C_{p,pred}$(MF)—calculated using parametrization given in Ref. [53]; $\Delta C_{p,pred}$(SLR)—calculated using parametrization given in Ref. [52]; $\Delta C_{p,pred}$(MSP)—calculated using parametrization given in Ref. [5]; $\Delta C_{p,pred}$(MP)—calculated using parametrization given in Ref. [42].

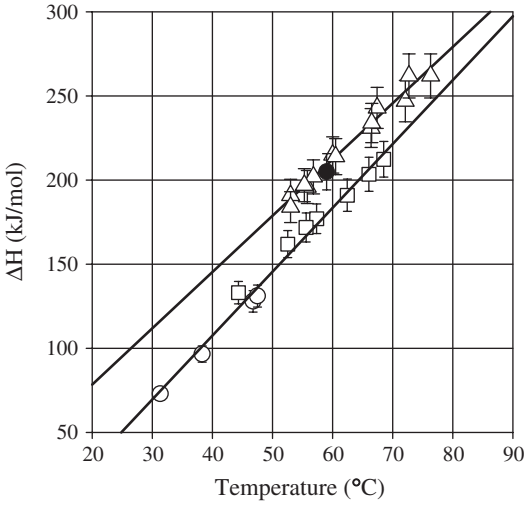

Fig. 7. Dependence of the enthalpy of unfolding on temperature. Experimental data for the WT^{AAA} (△), $34P^{AAA}$ (○), and $34P^{\#AAA}$ (□) ubiquitin variants and their linear fit (solid line). The data point for the WT protein (●) taken from Ref. [1] is also shown for comparison. The slopes represent the heat capacity change upon unfolding (ΔC_p) and are estimated to be 3.3±0.3, 3.2±0.4 and 3.5±0.4 kJ/(mol K), for the WT^{AAA}, $34P^{\#AAA}$, and $34P^{AAA}$ variants, respectively.

Since packing interactions in the native state are one of the major contributors to the positive enthalpy of protein unfolding, any decrease in packing should result in a decrease in the enthalpy of unfolding [42–44]. Hydrogen bonding also contributes positively to the enthalpy change upon unfolding [42,43]. The observed loss in hydrogen bonding for part of the helix in the 34P variant, is thus expected to reduce the enthalpy of unfolding [45–49].

Enthalpy changes are arguably difficult to predict accurately from a structure. There is, however, a general belief that even if these parameters cannot be predicted from the 3D-structures, their temperature dependencies, i.e. the heat capacity change upon unfolding, ΔC_p, can be quantitatively predicted. Indeed, experimental and semiempirical analysis by several groups have shown that ΔC_p for protein unfolding is well predicted based on the amount of solvent-exposed surface area upon unfolding [5,50–53] (but also see e.g. Ref. [10]). For a number of proteins, a simple equation has excellent prediction power for the experimental ΔC_p values:

$$\Delta C_{p,pred}\Delta = ASA_{npol} \cdot \Delta\bar{c}_{p,npol} + \Delta ASA_{pol} \cdot \Delta\bar{c}_{p,npol} \quad (2)$$

with ΔASA_{npol} and ΔASA_{pol} as the nonpolar and polar surface area changes upon unfolding, and $\Delta\bar{c}_p$,npol and $\Delta\bar{c}_p$,pol the heat capacity changes of a unit of surface area for nonpolar and polar groups, respectively. Values of $\Delta\bar{c}_p$,npol and $\Delta\bar{c}_p$,pol were parameterized using different approaches by different groups [5,50–53]. The experimentally determined heat capacity change for WT ubiquitin is 3.3±0.3 kJ/(mol K), statistically similar to the calculated values in heat capacity changes using differently derived parameters for Eq. (2), such as $\Delta C_{p,pred}$(SLR)=3.5±0.2 kJ/(mol K), $\Delta C_{p,pred}$(MSP)=3.4±0.1 kJ/(mol K) or $\Delta C_{p,pred}$(MP)=3.9±0.3 kJ/(mol K) (see Table 2). Interestingly, calculations failed to predict the heat capacity change for the 34P protein: according to the Eq. (2) ΔC_p for the $34P^{AAA}$ variant should be significantly smaller (Table 2), whereas within experimental error *no* changes in ΔC_p are observed experimentally (Figs. 3 and 7 and Table 2).

The large solvent-exposed hydrophobic crevice in the structure of the 34P variant, has seemingly no influence on the ΔC_p of unfolding for this protein, compared to the WT protein (Table 2). To further probe into the significance and/or nature of the hydrophobic crevice in the 34P structure additional experiments were carried out.

First, we compared the *m*-values derived from denaturant induced unfolding profiles. It is widely accepted that the dependence of the Gibbs energy on denaturant concentration, the *m*-value, reflects the amount of ASA exposed to solvent upon unfolding [54,55]. Furthermore, extensive correlation analysis supports this notion [5]. Fig. 8 compares the urea-induced unfolding profiles for the $34P^{\#AAA}$ and $34A^{AAA}$ variants. Analysis of the data according to the linear extrapolation model yields *m*-values of 6000±500 J/mol^2 and 6300±600 J/mol^2 for $34P^{\#AAA}$ and $34A^{AAA}$, respectively. The magnitude of these *m*-values is what expected for a protein of the size of ubiquitin under our experimental conditions [5,56]. The high degree of similarity for the *m*-values for the $34P^{\#AAA}$ and $34A^{AAA}$ variants suggests that upon unfolding, both variants expose similar amounts of surface area to solvent upon unfolding, consistent with the conclusion reached from the ΔC_p analysis.

Second, we compared ANS (8-anilino-1-naphthalene sulfonic acid) binding to the ubiquitin variants. ANS is known to interact with nonpolar surfaces in proteins and this binding is accompanied by a large increase in fluorescence, thereby providing a useful tool for detecting hydrophobic patches (see e.g. Refs. [57–59], but also see Ref. [60] suggesting electrostatic interactions). Fig. 9 shows the results of ANS fluorescence experiments for several 34P variants. As controls, we also performed similar experiments with other ubiquitin

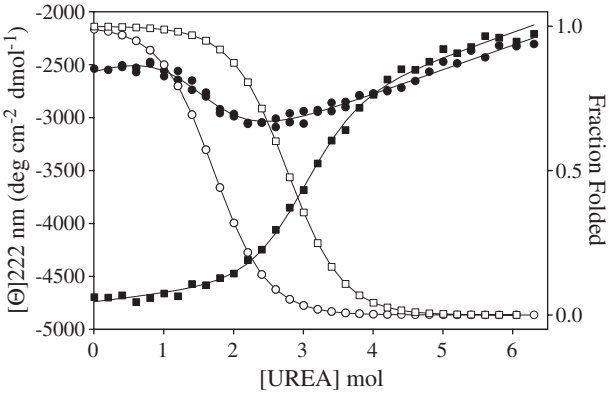

Fig. 8. Comparison of the urea induced unfolding for the $34P^{AAA}$ (○, ●) and $34P^{\#AAA}$ (□, ■) ubiquitin variants. Solid symbols are for the *y*-axes on the left that show the absolute values of ellipticity at 222 nm, open symbols are for the *y*-axes on the right that show the value expressed in fraction of native protein. Solid lines represent the fit of the experimental data to a two-state linear extrapolation model.

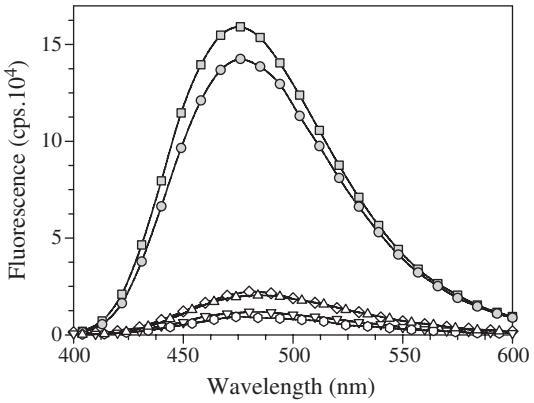

Fig. 9. ANS binding to several ubiquitin variants. Fluorescence emission spectra of ANS (10 μM) in the presence of $34P^{\#AA}A$ (●), $34P^{AAA}$ (■), $34A^{AAA}$ (△), $34E^{AAA}$ (▽), $34K^{AAA}$ (◇), $34L^{AAA}$ (○) (25 μM protein) at 25 °C in 25 mM sodium acetate, pH 5.5. ANS fluorescence in buffer alone was subtracted from all spectra.

variants, selected based on their overall stabilities ($34L^{AAA}$ is the most stable and 34K is the least stable protein), difference in charge at position 34 ($34K^{AAA}$ and $34E^{AAA}$) and the size of hydrophobic side chain in this position ($34L^{AAA}$ and $34A^{AAA}$). It is remarkable that the ANS fluorescence increase was only observed for 34P variants, and that this effect was independent of the background in which the substitution was made (i.e. $34P^{AAA}$ or $34P^{\#AAA}$). For all the control proteins ($34A^{AAA}$, $34L^{AAA}$, $34K^{AAA}$, $34E^{AAA}$) none, or very minor changes in ANS fluorescence intensity were observed (Fig. 9). This data indicates that only the 34P variants contain an accessible hydrophobic surface or patch that can bind the ANS fluorescence dye.

Given the above results, we have to reconcile the fact that the heat capacity changes and *m*-values for the $34P^{AAA}$ or $34P^{\#AAA}$ variants are essentially identical to those observed for WT ubiquitin or other position 34 variants, although local melting and/or local exposure of a hydrophobic area is observed in the structural (NMR, CD and ANS-binding) studies. One possibility is that ΔC_p and *m*-value measurements are indirect thermodynamic probes for the ΔASA estimates. Moreover, their relationship is inferred from the correlation analysis using well packed, natively folded proteins, and thus may be only strictly apply in these cases. Another possible explanation may be related to the nature of the structural change. Melting of a helical turn does not result in "complete" unfolding of the helix, it simply increases the local dynamics, resulting in the disappearance of close contacts, i.e. the NOE with amide protons of residues 12–16 and other residues. The disappearance of these NOEs can be caused by an increase in the "average" distance and, as a consequence, an appearance of the exposed hydrophobic cleft. On the other hand, the increase in "average" distance may simply be the result of increases in dynamic fluctuations, both on a spatial as well as frequency scale. As a result, NOEs between amide protons of residues 12–16 and those in the 27–34 amino acid segment will be severely attenuated, even if the average structure will exhibit only little change from the wild-type one. Such a dynamic, closed structural model would be consistent with the results of ΔC_p and *m*-value measurements, which suggest that the surface area change upon unfolding is not dramatically affected by the 34P substitution. The dynamic nature of the polypeptide chain around residue 34, will provide for easy access of ANS which binds to the transiently exposed hydrophobic residues in the 34P variants. This will be similar to the effects observed for example for IFABP in which hydrophobic ligand (including ANS) binding is gated by a helix, removal of which dramatically accelerates the binding kinetics.

The following model reconciles all the experimental data (NMR, DSC, fluorescence and CD) for the structure of the 34P variants: the overall structure is very similar to that of wild type ubiquitin, with the exception of residues in the last two turns of the helix (residues 27–33 in the wild type ubiquitin). These residues are no longer helical and this region of the polypeptide chain exhibits increased dynamics. The increase in the local motion, both in amplitude and frequency, allows transient opening of the hydrophobic core of the protein, as evidenced by the ability of the 34P variants to bind ANS. The hydrophobic core itself seems to be somewhat less well packed resulting in the lower enthalpy of unfolding of 34P variants. However, despite the increased mobility of the 27–33 region, the overall amount of buried surface area in the 34P proteins appears similar to that of the wild type, consistent with the similarities in of ΔC_p and *m*-values for these two ubiquitin variants.

4. Concluding remarks

An interesting result that emerged from our study concerns the cooperativity of protein unfolding. The thermal unfolding of WT ubiquitin is highly cooperative and follows apparent two-state behavior, a property characteristic for most small globular proteins [61]. For the 34P variants, a local secondary structure change and observed increased flexibility of this region is accompanied by a substantial decrease in stability. Nevertheless, the thermal unfolding of the 34P variant remains highly cooperative and follows an apparent two-state transition model. It appears that the C-terminus of the α-helix and its associated interactions with the remainder of the ubiquitin molecule can "melt" independently of the rest of the structure, without affecting the overall structural integrity and cooperative nature of unfolding. Such local unfolding of the C-terminus of α-helix in ubiquitin, although on a smaller scale, has been observed at elevated hydrostatic pressure [39] and in other small proteins [38].

Another interesting observation can be derived from comparison with previous kinetic studies of ubiquitin folding that identified the α-helix formation and its interactions with the first two β-strands as a obligatory step in the formation of the transition state ensemble [62–64]. The fact that in 34P variant the C-terminus of the α-helix is largely unstructured implies that the 34P variant probably forms a different transition state and consequently exhibits a very different energy landscape. Probing this folding landscape may constitute an interesting future study.

Acknowledgements

We thank Drs. D. Garrett and F. Delaglio for software, J. Baber for technical support and Dr. M. Lopez for the comments on the manuscript. This work was supported, in part, by the Intramural AIDS Targeted Antiviral Program of the Office of the Director of the National Institute of Health (to A. M.G.) and by a National Institutes of Health Grant GM54537 (to G.I.M.).

Appendix A. Supplementary data

Supplementary data associated with this article can be found, in the online version, at doi:10.1016/j.bpc.2006.03.017.

References

[1] D.N. Ermolenko, S.T. Thomas, R. Aurora, A.M. Gronenborn, G.I. Makhatadze, Hydrophobic interactions at the Ccap position of the C-capping motif of alpha-helices, J. Mol. Biol. 322 (2002) 123–135.
[2] S.T. Thomas, V.V. Loladze, G.I. Makhatadze, Hydration of the peptide backbone largely defines the thermodynamic propensity scale of residues at the C′ position of the C-capping box of alpha-helices, Proc. Natl. Acad. Sci. U. S. A. 98 (2001) 10670–10675.
[3] R. Aurora, G.D. Rose, Helix capping, Protein Sci. 7 (1998) 21–38.
[4] G.I. Makhatadze, V.V. Loladze, D.N. Ermolenko, X. Chen, S.T. Thomas, Contribution of surface salt bridges to protein stability: guidelines for protein engineering, J. Mol. Biol. 327 (2003) 1135–1148.
[5] J.K. Myers, C.N. Pace, J.M. Scholtz, Denaturant m values and heat capacity changes: relation to changes in accessible surface areas of protein unfolding, Protein Sci. 4 (1995) 2138–2148.
[6] M.M. Lopez, G.I. Makhatadze, Differential scanning calorimetry, Methods Mol. Biol. 173 (2002) 113–119.
[7] A.V. Gribenko, G.I. Makhatadze, Oligomerization and divalent ion binding properties of the S100P protein: a Ca2+/Mg2+-switch model, J. Mol. Biol. 283 (1998) 679–694.
[8] M.M. Lopez, K. Yutani, G.I. Makhatadze, Interactions of the major cold shock protein of *Bacillus subtilis* CspB with single-stranded DNA templates of different base composition, J. Biol. Chem. 274 (1999) 33601–33608.
[9] A.V. Gribenko, M. Guzman-Casado, M.M. Lopez, G.I. Makhatadze, Conformational and thermodynamic properties of peptide binding to the human S100P protein, Protein Sci. 11 (2002) 1367–1375.
[10] V.V. Loladze, D.N. Ermolenko, G.I. Makhatadze, Heat capacity changes upon burial of polar and nonpolar groups in proteins, Protein Sci. 10 (2001) 1343–1352.
[11] A. Bax, S. Grzesiek, Methodological advances in protein NMR, Accounts Chem. Res. 26 (1993) 131–138.
[12] S.W. Fesik, E.R. Zuiderweg, Heteronuclear three-dimensional NMR spectroscopy of isotopically labelled biological macromolecules, Q. Rev. Biophys. 23 (1990) 97–131.
[13] T.M. Logan, E.T. Olejniczak, R.X. Xu, S.W. Fesik, Side chain and backbone assignments in isotopically labeled proteins from two heteronuclear triple resonance experiments, FEBS Lett. 314 (1992) 413–418.
[14] D. Marion, P.C. Driscoll, L.E. Kay, P.T. Wingfield, A. Bax, A.M. Gronenborn, G.M. Clore, Overcoming the overlap problem in the assignment of 1H NMR spectra of larger proteins by use of three-dimensional heteronuclear 1H–15N Hartmann–Hahn-multiple quantum coherence and nuclear Overhauser-multiple quantum coherence spectroscopy: application to interleukin 1beta, Biochemistry 28 (1989) 6150–6156.
[15] G.M. Clore, A. Bax, P.C. Driscoll, P.T. Wingfield, A.M. Gronenborn, Assignment of the side-chain 1H and 13C resonances of interleukin-1 beta using double- and triple-resonance heteronuclear three-dimensional NMR spectroscopy, Biochemistry 29 (1990) 8172–8184.
[16] G.M. Clore, A.M. Gronenborn, Structures of larger proteins in solution: three- and four-dimensional heteronuclear NMR spectroscopy, Science 252 (1991) 1390–1399.
[17] M. Ruckert, G. Otting, Alignment of biological macromolecules in novel nonionic liquid crystalline media for NMR experiments, J. Am. Chem. Soc. 122 (2000) 7793–7797.
[18] J.J. Chou, S. Gaemers, B. Howder, J.M. Louis, A. Bax, A simple apparatus for generating stretched polyacrylamide gels, yielding uniform alignment of proteins and detergent micelles, J. Biomol. NMR 21 (2001) 377–382.
[19] K. Ding, A.M. Gronenborn, Sensitivity-enhanced E.COSY-type HSQC experiments for accurate measurements of one-bond 15N–1H(N) and 15N–13C′ and two-bond 13C′–1H(N) residual dipolar couplings in proteins, J. Magn. Reson. 158 (2002) 173–177.
[20] AT. Brunger, P.D. Adams, G.M. Clore, W.L. DeLano, P. Gros, R.W. Grosse-Kunstleve, J.S. Jiang, J. Kuszewski, M. Nilges, N.S. Pannu, R.J. Read, L.M. Rice, T. Simonson, G.L. Warren, Crystallography and NMR system: a new software suite for macromolecular structure determination, Acta Crystallogr., D Biol. Crystallogr. 54 (Pt 5) (1998) 905–921.
[21] M. Zweckstetter, A. Bax, Prediction of sterically induced alignment in a dilute liquid crystalline phase: aid to protein structure determination by NMR, J. Am. Chem. Soc. 122 (2000) 3379–3791.
[22] L.E. Kay, D.A. Torchia, A. Bax, Backbone dynamics of proteins as studied by 15N inverse detected heteronuclear NMR spectroscopy: application to staphylococcal nuclease, Biochemistry 28 (1989) 8972–8979.
[23] N.A. Farrow, O. Zhang, J.D. Forman-Kay, L.E. Kay, Characterization of the backbone dynamics of folded and denatured states of an SH3 domain, Biochemistry 36 (1997) 2390–2402.
[24] D. Garrett, R. Powers, A.M. Gronenborn, G.M. Clore, A common sense approach to peak picking in two-, three- and four-dimensional spectra using automatic computer analysis of contour diagrams. J. Magn. Reson. 95 (1991) 214–220.
[25] N. Tjandra, H. Kuboniwa, H. Ren, A. Bax, Rotational dynamics of calcium-free calmodulin studied by 15N-NMR relaxation measurements, Eur. J. Biochem. 230 (1995) 1014–1024.
[26] D.S. Wishart, B.D. Sykes, F.M. Richards, The chemical shift index: a fast and simple method for the assignment of protein secondary structure through NMR spectroscopy, Biochemistry 31 (1992) 1647–1651.
[27] G. Cornilescu, F. Delaglio, A. Bax, Protein backbone angle restraints from searching a database for chemical shift and sequence homology, J. Biomol. NMR 13 (1999) 289–302.
[28] N. Guex, M.C. Peitsch, SWISS-MODEL and the Swiss-PdbViewer: an environment for comparative protein modeling, Electrophoresis 18 (1997) 2714–2723.
[29] R.A. Laskowski, J.A. Rullmannn, M.W. MacArthur, R. Kaptein, J.M. Thornton, AQUA and PROCHECK-NMR: programs for checking the quality of protein structures solved by NMR, J. Biomol. NMR 8 (1996) 477–486.
[30] R. Koradi, M. Billeter, K. Wuthrich, MOLMOL: a program for display and analysis of macromolecular structures, J. Mol. Graph. 14 (1996), 51–55, 29–32.
[31] S.J. Hubbard, J.M. Thornton, 'NACCESS', Computer Program Department of Biochemistry and Molecular Biology, University College London, 1993.
[32] C. Chothia, Hydrophobic bonding and accessible surface area in proteins, Nature 248 (1974) 338–339.
[33] S. Kumar, M. Bansal, Dissecting alpha-helices: position-specific analysis of alpha-helices in globular proteins, Proteins 31 (1998) 460–476.
[34] S. Penel, E. Hughes, A.J. Doig, Side-chain structures in the first turn of the alpha-helix, J. Mol. Biol. 287 (1999) 127–143.
[35] P.R. Schimmel, P.J. Flory, Conformational energies and configurational statistics of copolypeptides containing L-proline, J. Mol. Biol. 34 (1968) 105–120.
[36] V.V. Loladze, B. Ibarra-Molero, J.M. Sanchez-Ruiz, G.I. Makhatadze, Engineering a thermostable protein via optimization of charge–charge interactions on the protein surface, Biochemistry 38 (1999) 16419–16423.

[37] A.M. Gronenborn, G.M. Clore, Rapid screening for structural integrity of expressed proteins by heteronuclear NMR spectroscopy, Protein Sci. 5 (1996) 174–177.
[38] K. Ding, J.M. Louis, A.M. Gronenborn, Insights into conformation and dynamics of protein GB1 during folding and unfolding by NMR, J. Mol. Biol. 335 (2004) 1299–1307.
[39] R. Kitahara, S. Yokoyama, K. Akasaka, NMR snapshots of a fluctuating protein structure: ubiquitin at 30 bar–3 kbar, J. Mol. Biol. 347 (2005) 277–285.
[40] E.C. Johnson, G.A. Lazar, J.R. Desjarlais, T.M. Handel, Solution structure and dynamics of a designed hydrophobic core variant of ubiquitin structure, Fold. Des. 7 (1999) 967–976.
[41] G.A. Lazar, J.R. Desjarlais, T.M. Handel, De novo design of the hydrophobic core of ubiquitin, Protein Sci. 6 (1997) 1167–1178.
[42] G.I. Makhatadze, P.L. Privalov, Energetics of protein structure, Adv. Protein Chem. 47 (1995) 307–425.
[43] T. Lazaridis, G. Archontis, M. Karplus, Enthalpic contribution to protein stability: insights from atom-based calculations and statistical mechanics, Adv. Protein Chem. 47 (1995) 231–306.
[44] V.V. Loladze, D.N. Ermolenko, G.I. Makhatadze, Thermodynamic consequences of burial of polar and non-polar amino acid residues in the protein interior, J. Mol. Biol. 320 (2002) 343–357.
[45] J.M. Scholtz, S. Marqusee, R.L. Baldwin, E.J. York, J.M. Stewart, M. Santoro, D.W. Bolen, Calorimetric determination of the enthalpy change for the alpha-helix to coil transition of an alanine peptide in water, Proc. Natl. Acad. Sci. U. S. A. 88 (1991) 2854–2858.
[46] M.M. Lopez, D.H. Chin, R.L. Baldwin, G.I. Makhatadze, The enthalpy of the alanine peptide helix measured by isothermal titration calorimetry using metal-binding to induce helix formation, Proc. Natl. Acad. Sci. U. S. A. 99 (2002) 1298–1302.
[47] J.M. Richardson, K.W. McMahon, C.C. MacDonald, G.I. Makhatadze, MEARA sequence repeat of human CstF-64 polyadenylation factor is helical in solution. A spectroscopic and calorimetric study, Biochemistry 38 (1999) 12869–12875.
[48] J.M. Richardson, G.I. Makhatadze, Temperature dependence of the thermodynamics of helix-coil transition, J. Mol. Biol. 335 (2004) 1029–1037.
[49] J.M. Richardson, M.M. Lopez, G.I. Makhatadze, Enthalpy of helix-coil transition: missing link in rationalizing the thermodynamics of helix-forming propensities of the amino acid residues, Proc. Natl. Acad. Sci. U. S. A. 102 (2005) 1413–1418.
[50] G.I. Makhatadze, P.L. Privalov, Heat capacity of proteins: I. Partial molar heat capacity of individual amino acid residues in aqueous solution: hydration effect, J. Mol. Biol. 213 (1990) 375–384.
[51] P.L. Privalov, G.I. Makhatadze, Heat capacity of proteins: II. Partial molar heat capacity of the unfolded polypeptide chain of proteins: protein unfolding effects, J. Mol. Biol. 213 (1990) 385–391.
[52] R.S. Spolar, J.R. Livingstone, M.T. Record Jr., Use of liquid hydrocarbon and amide transfer data to estimate contributions to thermodynamic functions of protein folding from the removal of nonpolar and polar surface from water, Biochemistry 31 (1992) 3947–3955.
[53] K.P. Murphy, E. Freire, Thermodynamics of structural stability and cooperative folding behavior in proteins, Adv. Protein Chem. 43 (1992) 313–361.
[54] J.A. Schellman, Solvent denaturation, Biopolymers 17 (1978) 1305–1322.
[55] D.O. Alonso, K.A. Dill, Solvent denaturation and stabilization of globular proteins, Biochemistry 30 (1991) 5974–5985.
[56] C.N. Pace, D.V. Laurents, J.A. Thomson, pH dependence of the urea and guanidine hydrochloride denaturation of ribonuclease A and ribonuclease T1, Biochemistry 29 (1990) 2564–2572.
[57] Y. Goto, T. Azuma, K. Hamaguchi, Refolding of the immunoglobulin light chain, J. Biochem. (Tokyo) 85 (1979) 1427–1438.
[58] J.R. Lakowitcz, Principles of Fluorescence Spectroscopy, Plenum Press, New York, 1983.
[59] C.M. Teschke, J. King, P.E. Prevelige Jr., Inhibition of viral capsid assembly by 1,1′-bi(4-anilinonaphthalene-5-sulfonic acid), Biochemistry 32 (1993) 10658–10665.
[60] D. Matulis, R. Lovrien, 1-Anilino-8-naphthalene sulfonate anion-protein binding depends primarily on ion pair formation, Biophys. J. 74 (1998) 422–429.
[61] P.L. Privalov, N.N. Khechinashvili, A thermodynamic approach to the problem of stabilization of globular protein structure: a calorimetric study, J. Mol. Biol. 86 (1974) 665–684.
[62] M.S. Briggs, H. Roder, Early hydrogen-bonding events in the folding reaction of ubiquitin, Proc. Natl. Acad. Sci. U. S. A. 89 (1992) 2017–2021.
[63] B.A. Krantz, R.S. Dothager, T.R. Sosnick, Discerning the structure and energy of multiple transition states in protein folding using psi-analysis, J. Mol. Biol. 337 (2004) 463–475.
[64] H.M. Went, S.E. Jackson, Ubiquitin folds through a highly polarized transition state, Protein Eng., Des. Sel. 18 (2005) 229–237.